HAL
open science

The perihelion activity of comet 67P/Churyumov-Gerasimenko as seen by robotic telescopes

Colin Snodgrass, Cyrielle Opitom, Miguel de Val-Borro, Emmanuel Jehin, Jean Manfroid, Tim Lister, Jon Marchant, Geraint H. Jones, Alan Fitzsimmons, Iain A. Steele, et al.

To cite this version:

Colin Snodgrass, Cyrielle Opitom, Miguel de Val-Borro, Emmanuel Jehin, Jean Manfroid, et al.. The perihelion activity of comet 67P/Churyumov-Gerasimenko as seen by robotic telescopes. Monthly Notices of the Royal Astronomical Society, 2016, 462 (Suppl. 1), pp.S138-S145. 10.1093/mnras/stw2300 . insu-01367573

HAL Id: insu-01367573

https://insu.hal.science/insu-01367573v1

Submitted on 22 Jun 2017

HAL is a multi-disciplinary open access archive for the deposit and dissemination of scientific research documents, whether they are published or not. The documents may come from teaching and research institutions in France or abroad, or from public or private research centers.

L'archive ouverte pluridisciplinaire **HAL**, est destinée au dépôt et à la diffusion de documents scientifiques de niveau recherche, publiés ou non, émanant des établissements d'enseignement et de recherche français ou étrangers, des laboratoires publics ou privés.

Monthly Notices of the ROYAL ASTRONOMICAL SOCIETY

MNRAS **462,** S138–S145 (2016)
Advance Access publication 2016 September 12

doi:10.1093/mnras/stw2300

The perihelion activity of comet 67P/Churyumov–Gerasimenko as seen by robotic telescopes

Colin Snodgrass,[1★] Cyrielle Opitom,[2] Miguel de Val-Borro,[3,4] Emmanuel Jehin,[2] Jean Manfroid,[2] Tim Lister,[5] Jon Marchant,[6] Geraint H. Jones,[7,8] Alan Fitzsimmons,[9] Iain A. Steele,[6] Robert J. Smith,[6] Helen Jermak,[6,10] Thomas Granzer,[11] Karen J. Meech,[12] Philippe Rousselot[13] and Anny-Chantal Levasseur-Regourd[14]

[1]*School of Physical Sciences, The Open University, Walton Hall, Milton Keynes MK7 6AA, UK*
[2]*Institut d'Astrophysique et de Géophysique, Université de Liège, allée du 6 Août 17, B-4000 Liège, Belgium*
[3]*Department of Astrophysical Sciences, Princeton University, Princeton, NJ 08544, USA*
[4]*NASA Goddard Space Flight Center, Astrochemistry Laboratory, Code 691.0, Greenbelt, MD 20771, USA*
[5]*Las Cumbres Observatory Global Telescope Network, 6740 Cortona Drive Ste. 102, Goleta, CA 93117, USA*
[6]*Astrophysics Research Institute, Liverpool John Moores University, Liverpool L3 5RF, UK*
[7]*Mullard Space Science Laboratory, University College London, Holmbury St. Mary, Dorking, Surrey RH5 6NT, UK*
[8]*The Centre for Planetary Sciences at UCL/Birkbeck, Gower Street, London WC1E 6BT, UK*
[9]*Astrophysics Research Centre, School of Mathematics and Physics, Queen's University Belfast, BT7 1NN, UK*
[10]*Physics Department, Lancaster University, Lancaster LA1 4YB, UK*
[11]*Leibniz-Institut für Astrophysik Potsdam, An der Sternwarte 16, D-14482 Potsdam, Germany*
[12]*Institute for Astronomy, 2680 Woodlawn Drive, Honolulu, HI 96822, USA*
[13]*University of Franche-Comté, Observatoire des Sciences de l'Univers THETA, Institut UTINAM – UMR CNRS 6213, BP 1615, F-25010 Besançon Cedex, France*
[14]*LATMOS-IPSL; UPMC (Sorbonne Univ.), BC 102, 4 place Jussieu, F-75005 Paris, France*

Accepted 2016 September 9. Received 2016 September 3; in original form 2016 July 10

ABSTRACT

Around the time of its perihelion passage, the observability of 67P/Churyumov–Gerasimenko from Earth was limited to very short windows each morning from any given site, due to the low solar elongation of the comet. The peak in the comet's activity was therefore difficult to observe with conventionally scheduled telescopes, but was possible where service/queue-scheduled mode was possible, and with robotic telescopes. We describe the robotic observations that allowed us to measure the total activity of the comet around perihelion, via photometry (dust) and spectroscopy (gas), and compare these results with the measurements at this time by Rosetta's instruments. The peak of activity occurred approximately two weeks after perihelion. The total brightness (dust) largely followed the predictions from Snodgrass et al., with no significant change in total activity levels from previous apparitions. The CN gas production rate matched previous orbits near perihelion, but appeared to be relatively low later in the year.

Key words: comets: individual: 67P/Churyumov–Gerasimenko.

1 INTRODUCTION

A large world-wide campaign of ground-based observations supported the European Space Agency's unique Rosetta mission, the first spacecraft to orbit a comet, which followed 67P/Churyumov–Gerasimenko (hereafter 67P) from 2014 to 2016 as it passed through perihelion. The campaign had the dual purpose of providing large-scale context for Rosetta, by measuring total production rates and observing the coma and tails beyond the spacecraft's orbit, and allowing comparison between 67P and other comets. Predictions for the total dust activity of the comet were made by Snodgrass et al. (2013), based on observations from previous orbits, and observations in the pre-landing phase of the mission showed the comet to be following these predictions (Snodgrass et al. 2016). This implies that there is little change from orbit to orbit in 67P, and that results from Rosetta can be more generally applied. A simple thermophysical model (balancing the sublimation needed to produce the observed dust coma with the input solar irradiance – e.g. Meech & Svoreň 2004) was able to describe most observations presented by Snodgrass et al. (2013), but underestimated the peak brightness relative to the data in the region around the perihelion passage. The peak in activity was also an important opportunity to measure the total gas production of the comet, after deep searches with large aperture

★ E-mail: colin.snodgrass@open.ac.uk

© 2016 The Authors
Published by Oxford University Press on behalf of the Royal Astronomical Society

Table 1. Log of observations described in this paper, together with heliocentric and geocentric distances (r and Δ, au) and solar phase angle (α, degrees). Dates are all 2015, format MM-DD.dd. TRAPPIST data. Full table is available online, first five rows given as an example.

UT date	Tel./inst.	$N \times t_{exp}$ filter	r	Δ	α
04-18.41	TRAPPIST	2 × 240 s Rc	1.83	2.64	15.6
04-25.42	TRAPPIST	3 × 180 s Rc	1.78	2.56	17.2
04-29.42	TRAPPIST	2 × 180 s Rc	1.75	2.51	18.1
05-04.42	TRAPPIST	1 × 180 s Rc	1.71	2.45	19.2
05-05.42	TRAPPIST	3 × 180 s Rc	1.71	2.44	19.5
...	...	...	...	...	...

telescopes could only produce upper limits to emissions in the 2014 observing window (Snodgrass et al. 2016). Good coverage of the perihelion passage was therefore a priority for the ground-based observation campaign, despite the challenging observing geometry.

67P was in southern skies during the 2014 observing window (February–November), and slowly brightened as it approached the Sun from ∼4–3 au, but still required large aperture telescopes to observe. After a gap in coverage enforced by low solar elongation between 2014 December and 2015 April, the comet was briefly observable from the Southern hemisphere before reaching declination of +24° around the time of its perihelion passage (2015 August). Throughout the perihelion period, the phase angle was around 30°, and the solar elongation varied from 30° to 90°, with the comet observable only in morning twilight for the majority of the time. At this time, smaller aperture robotic telescopes were better able to follow the comet than the larger facilities used in 2014.

In this paper, we describe observations taken as part of an International Time Programme (ITP) using Canary Island telescopes, the 2-m Liverpool Telescope (LT) on La Palma and the 1.2-m STELLar Activity (STELLA) imaging telescope on Tenerife, and with the specialist comet observing 0.6-m TRAnsiting Planets and Planetesimals Small Telescope (TRAPPIST), at La Silla in Chile, and the robotic telescopes operated by Las Cumbres Observatory Global Telescope Network (LCOGT). Observations in the months around perihelion (2015 August 13) are included in the current work, corresponding to the period when the peak in activity was observed, while the comet was at heliocentric distances $1.2 < r < 2$ au. The following section describes the observations from each telescope, while Section 3 reports the total activity measurements derived. We discuss the implications of these results, and compare them with earlier observations and Rosetta measurements, in Section 4.

2 OBSERVATIONS

We summarize the observations around perihelion in Table 1, and describe them in more detail in the following sub-sections.

2.1 TRAPPIST

TRAPPIST is a 60-cm robotic telescope installed in 2010 at La Silla observatory (Jehin et al. 2011). The telescope is equipped with a 2K × 2K thermoelectrically cooled Finger Lakes Instrumentation Proline CCD camera with a field of view of 22 arcmin × 22 arcmin. We binned the pixels 2 × 2 and obtained a resulting plate scale of 1.3 arcsec pixel^{-1}. The telescope is equipped with a set of narrow-band filters designed for the observing campaign of comet Hale–Bopp (Farnham, Schleicher & A'Hearn 2000) isolating the emission of OH, NH, CN, C_3, C_2 and emission-free continuum regions at four wavelengths. A set of broad-band B, V, Rc and Ic Johnson–Cousin filters is also mounted on the telescope. We observed the comet once or twice a week from 2015 April 18 to the end of the year, with broad-band filters. Exposure times ranged from 120 to 240 s. Technical problems and bad weather prevented observations for some days around perihelion. Between 2015 August 22 and 2015 September 12, we were able to detect the CN emission using narrow-band filters. The C_2 was also detected but the signal-to-noise ratio (SNR) was not sufficient to derive reliable gas production rates. We could not detect the OH, NH or C_3 emission. Upper limits on the production rates for gas species other than CN have not yet been derived, but will be presented as part of a more in-depth study of using TRAPPIST and VLT data (Opitom et al., in preparation) .

Table 2. CN production rates measured by TRAPPIST and LOTUS.

UT date 2015	Tel./inst.	r (au)	Δ (au)	Q(CN) molec. s^{-1}
08-22.43	TRAPPIST	1.25	1.77	$6.72 \pm 0.64 \times 10^{24}$
08-24.42	TRAPPIST	1.25	1.77	$7.77 \pm 0.82 \times 10^{24}$
08-29.42	TRAPPIST	1.26	1.77	$1.00 \pm 0.10 \times 10^{25}$
09-11.41	TRAPPIST	1.29	1.78	$8.45 \pm 0.93 \times 10^{24}$
09-12.41	TRAPPIST	1.30	1.78	$7.49 \pm 0.91 \times 10^{24}$
09-05.24	LT/LOTUS	1.28	1.77	$8.74 \pm 0.70 \times 10^{24}$
09-10.24	LT/LOTUS	1.29	1.78	$8.93 \pm 0.74 \times 10^{24}$
09-15.23	LT/LOTUS	1.31	1.78	$7.62 \pm 0.78 \times 10^{24}$
09-30.24	LT/LOTUS	1.37	1.80	$5.47 \pm 0.82 \times 10^{24}$
10-07.23	LT/LOTUS	1.41	1.80	$2.83 \pm 0.86 \times 10^{24}$
10-13.24	LT/LOTUS	1.45	1.81	$3.23 \pm 0.90 \times 10^{24}$
10-26.22	LT/LOTUS	1.53	1.81	$2.06 \pm 0.94 \times 10^{24}$
11-03.25	LT/LOTUS	1.58	1.80	$1.14 \pm 0.98 \times 10^{24}$
11-08.23	LT/LOTUS	1.62	1.80	$2.37 \pm 1.02 \times 10^{24}$
11-10.24	LT/LOTUS	1.63	1.79	$9.44 \pm 9.06 \times 10^{23}$
11-12.21	LT/LOTUS	1.64	1.79	$5.90 \pm 5.10 \times 10^{23}$
11-14.26	LT/LOTUS	1.66	1.79	$9.82 \pm 9.14 \times 10^{23}$
12-03.22	LT/LOTUS	1.80	1.74	$3.42 \pm 3.18 \times 10^{23}$
12-10.28	LT/LOTUS	1.85	1.72	$1.40 \pm 1.22 \times 10^{24}$

Calibration followed standard procedures using frequently updated master bias, flat and dark frames. The removal of the sky contamination and the flux calibration were performed as described in Opitom et al. (2015). Median radial profiles were extracted from each image and dust contamination was removed from the CN profiles. Observations in the Rc broad-band filter were used to derive total R-band magnitudes at 10 000 km. We also derived the $Af\rho$ at 10 000 km and corrected it from the phase angle effect using a function that is a composite of two different phase functions from Schleicher, Millis & Birch (1998) and Marcus (2007). From the observations in the CN narrow-band filter, we derived CN production rates. The CN fluxes were converted into column density and we adjusted a Haser model (Haser 1957) on the profiles to derive the production rates (Table 2). The model adjustment was performed around a physical distance of 10 000 km from the nucleus to avoid point spread function and seeing effects around the optocentre and low SNR at larger nucleocentric distances. We used a constant outflow velocity of 1 km s^{-1} as assumed by A'Hearn et al. (1995), together with their scalelengths scaled as r^2, r being the heliocentric distance.

2.2 Liverpool telescope

The 2-m LT was one of the first fully robotic professional telescopes, and has been in operation at Roque de los Muchachos Observatory on La Palma since 2003. It was built and is operated by Liverpool John Moores University, and is equipped with an array of instruments (imagers, spectrographs and polarimeters) that can

be quickly switched between during the night (Steele et al. 2004). As one of the larger telescopes that could regularly observe 67P around perihelion, we proposed to use it primarily for spectroscopy, to study the dust colours (continuum slope) and gas emission bands. As the existing long-slit spectrograph, SPectrograph for the Rapid Acquisition of Transients (Piascik et al. 2014), covers red wavelengths where cometary gasses have only weaker emissions, the LT team proposed the creation of a new low-resolution ($R \sim 330$) blue/ultraviolet (UV) (320–630 nm) sensitive spectrograph for the 67P monitoring programme. The rapid design, construction and commissioning of this instrument, the LOw-cosT Ultraviolet Spectrograph (LOTUS), enabled us to observe the stronger CN band at 388 nm (Steele et al. 2016).

Observations of 67P using LOTUS began on 2015 September 5 and continued until the comet had faded too far for UV spectroscopy with the LT. LOTUS was designed with a two-width slit, the longer and narrower part slit of 2.5 arcsec × 95 arcsec being optimized for comet observations, while the wider 5 arcsec × 25 arcsec slit allowed observations of spectrophotometric standard stars to measure the instrument response. The CCD pixels were binned 4 × 4 to obtain a spatial pixel scale of 0.6 arcsec pixel^{-1}.

LOTUS spectroscopic data were reduced with the routine pipeline to produce science frames. This pipeline is based on the Fibre-fed RObotic Dual-beam Optical Spectrograph (FRODOSpec) reduction pipeline (Barnsley, Smith & Steele 2012) and is similar to that of other long-slit instruments. First, the bias and dark frames were subtracted and the wavelength calibration carried out. The pipeline automatically aligns the dispersion direction in the two-dimensional frames with rows of the array to produce wavelength calibrated spectra. Three 300-s comet spectra obtained for each epoch were median combined and extracted by summing the flux over an aperture along the slit. Several frames with clean sky background were observed at the same airmass to perform the sky subtraction for each combined frame. Finally, the spectra of the comet were corrected for atmospheric extinction and flux calibrated with observations of standard star using standard IRAF techniques. The continuum in the comet spectra caused by sunlight reflection off the dust was removed using the spectrum of the solar analogue HD 29641 that was observed in the beginning of the observing period.

From the LOTUS observations, we derived CN production rates using a Haser spherically symmetric model (Haser 1957) that is also used for the analysis of the TRAPPIST photometric data described in Section 2.1. We included the photoproduction and dissociation of molecules in the coma with parent and daughter scalelengths and fluorescence efficiencies taken from Schleicher (2010). With this model, the column density in a circular area of the observed species is proportional to the measured flux of the emission band, from which the production rate can be derived directly.

There were also images of the comet collected with the LT, using its IO:O camera (Steele et al. 2014). These include the acquisition images taken to robotically acquire the comet on to the slit of LOTUS, and some additional deeper images. Images were mostly taken in the SDSS-*r* filter, with additional sets in *griz* taken to measure the colour of the coma in the weeks closest to perihelion. All images taken with the LT were processed using the IO:O pipeline, which performs bias subtraction, flat-fielding and photometric calibration.

2.3 STELLA

The STELLA telescopes are a pair of 1.2-m telescopes at the Teide observatory on the island of Tenerife, built and operated by the Leibniz-Institut für Astrophysik Potsdam (AIP) in collaboration with the Instituto de Astrofísica de Canarias (IAC). The pair of telescopes have complementary instrumentation – a wide-field imager on one telescope and high-resolution spectrograph on the other – and were built with monitoring of stellar activity in cool stars in mind. Further details on the telescopes can be found in the papers by Strassmeier et al. (2010, 2004).

We used the imaging telescope to perform imaging in an SDSS-*r* filter on every possible night, and attempted *griz* filter observations every 10 nights. The instrument, the Wide Field STELLA Imaging Photometer, has a 22 arcmin field of view and 0.32 arcsec pixel^{-1} pixel scale, using a single 4K CCD. The STELLA telescope telescope control system does not allow tracking of moving (Solar system) objects, and expects a fixed RA and Dec. for each target. Observing blocks (OBs) are created and submitted to the queue using a JAVA tool. In order to interact with this system, creation of the OBs was scripted to produce one block per night with appropriate start and end time constraints, the correct position and a short enough exposure time that the comet would not move more than 0.5 arcsec during the exposure (and therefore stay within the seeing disc). The number of exposures was scaled to have an approximately fixed OB length (10 min in the near-perihelion period). These OBs were then inserted directly into the telescope queue.

Data were taken robotically and automatically reduced using the STELLA pipeline, which also determines individual frame zero-points by matching field stars with the PPMXL catalogue (Roeser, Demleitner & Schilbach 2010). This is based on USNO-B1.0 and 2MASS catalogues; transformations from Bilir et al. (2008) and Jester et al. (2005) are used to give zero-points in the SDSS-like filters. The resulting absolute calibration is internally consistent, as can be seen by the smooth night-to-night variation, and gives a good match in the *r* band to other total brightness values from other telescopes, but the filter-to-filter zero-points are not well calibrated, and therefore further calibration is required to measure the colour of the comet using the STELLA data.

The resulting frames for each night were shifted and stacked, based on the predicted motion of the comet, to produce one median image per filter and night. These were inspected visually to confirm that the comet was detected, and remove any nights where the comet fell on top of a star or there were issues with the data quality. There were occasionally problems with the telescope focus, which is automatic but did not always perform well at the low elevation the telescope needed to point to for observations of 67P. Badly defocussed images were rejected. The total comet brightness was then measured within various apertures – here we report the brightness within $\rho = 10\,000$ km at the distance of the comet.

2.4 LCOGT

LCOGT is a global network of robotic telescopes designed for the study of time-domain phenomena on a variety of time-scales. The LCOGT network incorporates the two 2-m Faulkes Telescopes (very similar to the LT described in Section 2.2) and nine 1-m telescopes deployed at a total of five locations around the world, and have been operating as a combined network since 2014 May. The LCOGT network is described in more detail in Brown et al. (2013) and the operation of the network is described in Boroson et al. (2014).

Due to the visibility of 67P, we started observations on 2015 August 7 with the 2-m Faulkes Telescope North on Haleakala, Maui, Hawaii using the fs02 instrument. This instrument is a Spectral Instruments 600 camera using a Fairchild 4096 × 4096 pixel CCD486

CCD that was operated in bin 2 × 2 mode to give a pixel scale of 0.3 arcsec pixel^{-1} and a field of view of 10 arcmin × 10 arcmin. Observations were primarily conducted in SDSS-g' and SDSS-r' but a series of $g'r'i'z'$ observations were taken on seven nights between 2015 September 3 and 2015 September 21.

Observations with the 1-m network started on 2015 December 8 and continued through until 2016 March 26 – in this paper, we describe data taken up to the end of 2015 December. Observations were obtained from the LCOGT sites at McDonald Observatory (Texas; one telescope), Cerro Tololo (Chile; three telescopes), Sutherland (South Africa; two telescopes) and Siding Spring Observatory (Australia; one telescope) and were all obtained in SDSS-r'. Two different instrument types were used; the first one uses a SBIG STX-16803 camera with a Kodak KAF-16803 CCD with 4096 × 4096 9 μm pixels that was operated in bin 2 × 2 mode to give a pixel scale of 0.464 arcsec pixel^{-1} and a field of view of 15.8 arcmin × 15.8 arcmin. The other instrument type was the LCOGT-manufactured Sinistro camera using a Fairchild 4096 × 4096 pixel CCD486 CCD that was operated in bin 1 × 1 mode to give a pixel scale of 0.387 arcsec pixel^{-1} and a field of view of 26.4 arcmin × 26.4 arcmin.

All data were reduced with the LCOGT Pipeline based on ORAC-DR (Jenness & Economou 2015 and also described in more detail in Brown et al. 2013) to perform the bad-pixel masking, bias and dark subtraction, flat-fielding, astrometric solution and source catalogue extraction. In order to produce a more consistent result and to allow the use of photometric apertures that are a fixed size at the distance of the comet (and therefore of variable size on the CCD), we elected to resolve the astrometric and photometric (zero-point determination) solution for all the data using a custom pipeline that operated on the results of the LCOGT Pipeline.

This comet-specific pipeline makes use of SEXTRACTOR (Bertin & Arnouts 1996) and SCAMP (Bertin 2006) to produce a source catalogue and solve for the astrometric transformation from pixel co-ordinates to RA, Dec. The UCAC4 catalogue (Zacharias et al. 2013) was used by SCAMP to determine the astrometric solution and also by the pipeline to determine the zero-point between the instrumental magnitudes and the magnitude for cross-matched sources in the UCAC4 catalogue. Outlier rejection was used to eliminate those cross-matches with errant magnitudes (in either the CCD frame or the UCAC4 catalogue) and this process was repeated until no more cross-matches were rejected. In a small number of cases, readout/shutter problems with the SBIG cameras caused part of the image to receive no light and the zero-point determination failed in these cases. The frames were excluded from the analysis.

The comet magnitudes were then measured through photometric aperture centred on the predicted position and with a radius corresponding to 10 000 km at the time of observation, taking into account the appropriate pixel scale of the instrument used and the Earth–comet distance. The predicted position and distance were interpolated for the mid-point of the observation in ephemeris output, produced by the JPL HORIZONS system (Giorgini 2015).

3 ACTIVITY MEASUREMENTS

3.1 Total brightness

Fig. 1 recreates the predicted apparent brightness of the comet from Snodgrass et al. (2013) (their fig. 10), with photometry from 2014 (Snodgrass et al. 2016) and this work overlaid. It can be seen that the total brightness of the comet, as measured in the R band within a $\rho = 10\,000$ km radius aperture, is in very good agreement with

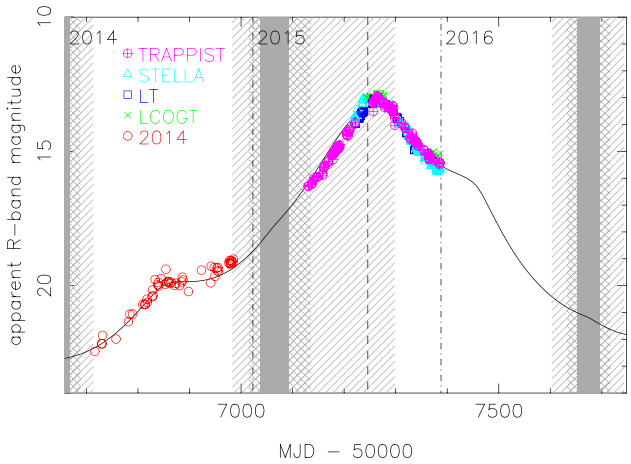

Figure 1. Prediction versus measurements of total R-band magnitude within $\rho = 10\,000$ km. Hatched, cross-hatched and solid shading show periods when the solar elongation is less than 50°, 30° and 15°, respectively. The vertical dashed line marks perihelion.

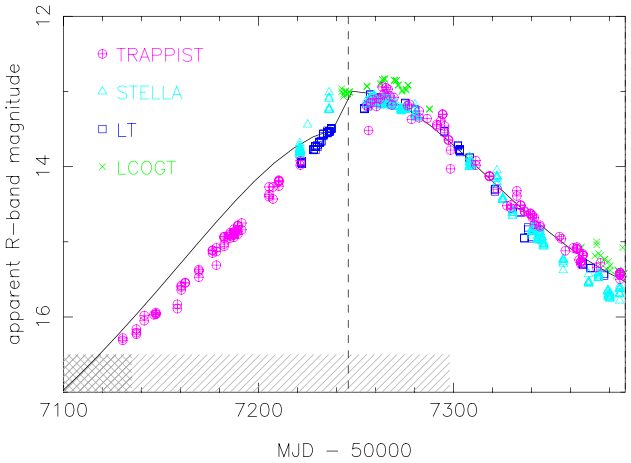

Figure 2. Same as Fig. 1, showing zoom in on 2015 period around perihelion. Here the solar elongation is shown by shading at the bottom of the plot only, for ease of seeing data points.

predictions throughout the current apparition. In this figure, and all subsequent ones, we have converted SDSS r' filter photometry to R band for ease of comparison with previous VLT FORS photometry and the Snodgrass et al. (2013) predictions. We use the conversion from Lupton,[1] $R = r - 0.1837(g - r) - 0.0971$, together with the $(g - r) = 0.62 \pm 0.04$ colour of the comet measured with the LT (see Section 3.2 below). We show a zoom in on the 2015 data ($r < 2$ au) in Fig. 2, which shows a number of features. First, the good agreement between the photometry with different telescopes and filters following the conversion to R band is clear. Secondly, there is an obvious offset in the peak brightness post-perihelion, and a strong asymmetry – the apparent magnitude of the comet is brighter at the same distances post-perihelion than pre-perihelion. Finally, it is also apparent that the photometry pre-perihelion is consistently fainter than the predicted curve, although it follows the same trend. Following the method used in Snodgrass et al. (2016),

[1] http://cas.sdss.org/dr6/en/help/docs/algorithm.asp?key=sdss2UBVRIT

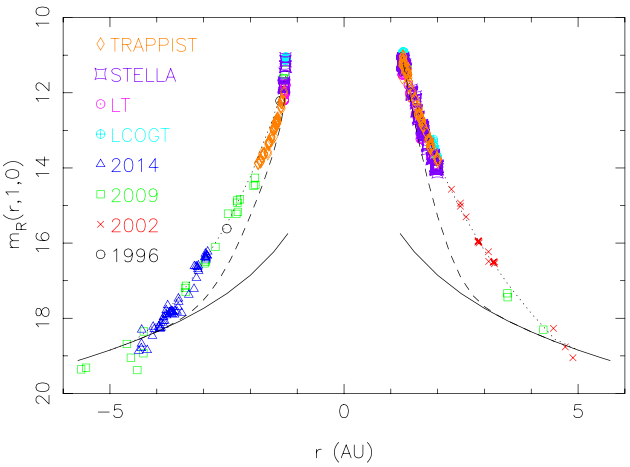

Figure 3. Total R-band magnitude within $\rho = 10\,000$ km, corrected to unit geocentric distance and 0°phase angle, against heliocentric distance. The solid line shows the predicted magnitude of the inactive nucleus, the dashed line a prediction based on the expected total water prediction rate and the dotted line an empirical prediction based on photometry from previous orbits (see Snodgrass et al. 2013, for details)

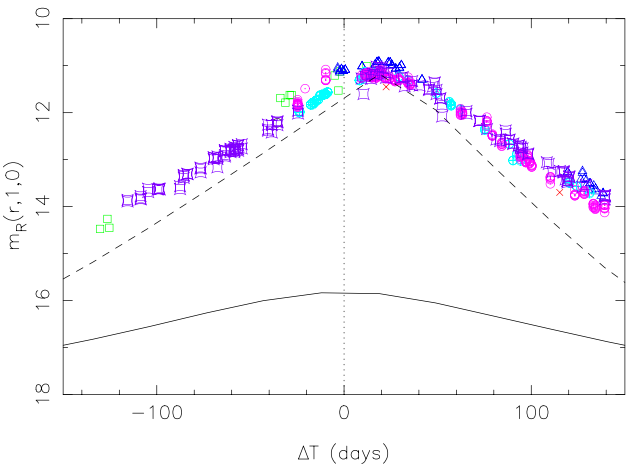

Figure 4. Same as Fig. 3, but plotted against time from perihelion (days) and showing only the near-perihelion period (± 150 d).

we find that this implies a drop in total activity in this period of 37 ± 9 per cent relative to previous orbits, but we caution that the empirical prediction is only meant to be approximate. The step in the prediction curve between pre- and post-perihelion models, for example, is not a real feature. The very good match to the prediction post-perihelion suggests that there is no significant difference in total activity levels in this apparition (difference in flux is 3 ± 9 per cent), and the smooth curve through the post-perihelion peak implies that the mismatch pre-perihelion is probably due to the simplification in the models (which are simple power-law fits to heliocentric distance pre- and post-perihelion).

In Figs 3 and 4, we plot the same photometry reduced to unit geocentric distance and zero phase angle, as a function of heliocentric distance and time from perihelion, respectively. We assume a linear phase function with $\beta = 0.02$ mag deg^{-1}, which is a good approximation for cometary dust (see discussion in Snodgrass et al. 2016). These plots show the data and models from Snodgrass et al. (2013, 2016) as well as the perihelion data, and show the consistency between the brightness of this apparition and previous orbits.

The total dust activity can also be expressed using the commonly used $Af\rho$ parameter (A'Hearn et al. 1984). We find that the comet peaked with $Af\rho \sim 400$ cm, or $Af\rho \sim 1000$ cm including a correction to zero phase angle, in the weeks after perihelion. Values for $Af\rho$ are given alongside the measured magnitudes in Table A1.

3.2 Colour of the coma

Using the observations from the LT, we derive average colours for the coma in SDSS bands: $(g - r) = 0.62 \pm 0.04$, $(r - i) = 0.11 \pm 0.03$ and $(i - z) = -0.45 \pm 0.04$. These are redder, approximately the same, and bluer than the Sun [$(g - r)_\odot = 0.45$, $(r - i)_\odot = 0.12$, $(i - z)_\odot = 0.04$ – Holmberg, Flynn & Portinari 2006, respectively. This follows the general pattern seen in earlier data, and observations from Rosetta, of the spectral slope being bluer at longer wavelengths (Capaccioni et al. 2015; Fornasier et al. 2015; Snodgrass et al. 2016), but the extremely blue $(i - z)$ colour is surprising. The calibration of this photometry is based on pipeline results, and the colour term found for calibration in the i and z filters is relatively uncertain, which could contribute some uncertainty – the individual measurements in $(r - i)$ and $(i - z)$ are more variable than the $(g - r)$ colour, which is very stable around the average value for all epochs. Consequently, we have more confidence in the $(g - r)$ colour, but regard the other colours as requiring confirmation based on direct calibration of the frames. This will be done with the forthcoming public release of all sky photometric catalogues in these bands (e.g. Pan-STARRS 1), which will allow direct calibration against field stars in each frame, as part of a more detailed study on the long-term evolution of the colours of the coma, including *griz* photometry from the LT, STELLA and LCOGT telescopes (to be published in a future paper). Finally, we note that the g-band brightness contains both dust continuum and C_2 (0−0) band emission so that the intrinsic dust $(g - r)$ colour will be slightly redder than measured, but our LOTUS spectra show this to be extremely weak.

3.3 Gas production

We can also assess the total activity of the comet in terms of gas production. From the ground it is difficult to assess the production rates of H_2O, CO or CO_2 that dominate the coma, so we have to make the assumption that more easily detected species are representative of the total gas production. Rosetta results show that the picture is more complicated (e.g. Le Roy et al. 2015; Luspay-Kuti et al. 2015), but a first-order assumption that more CN, for example, implies more total gas is probably still valid.

We show an example of LOTUS spectrum in Fig. 5. Emission from CN was detected with LOTUS at 3880 Å, as well as several spectral features due to C_2 emission at 4738, 5165and 5635 Å. The strongest feature, CN, was detectable from perihelion until the end of 2015, at nearly 2 au. We were also able to detect CN at a handful of epochs close to perihelion using narrow-band photometry with TRAPPIST, but the comet was too faint (and too low elevation when viewed from Chile) to follow its production rate over an extended period via photometry.

Fig. 6 shows the CN production rates as a function of heliocentric distance obtained with LOTUS and TRAPPIST. The measurements from the different telescopes and techniques are in good agreement during the period when they overlap. The total CN production rate falls off slowly with increasing heliocentric distance, noticeably

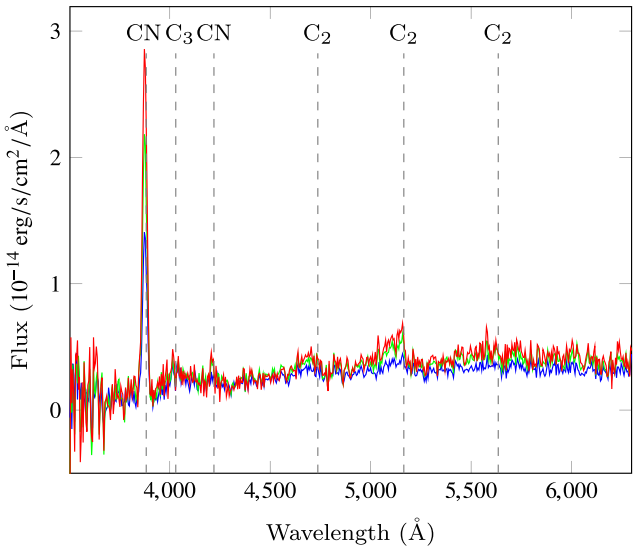

Figure 5. Sky-subtracted spectra of comet 67P obtained on September 5 with LOTUS. The spectra are extracted at three different apertures centred on the comet nucleus with diameters 8.4 (blue line), 16.8 (green line) and 33.6 arcsec (red line).

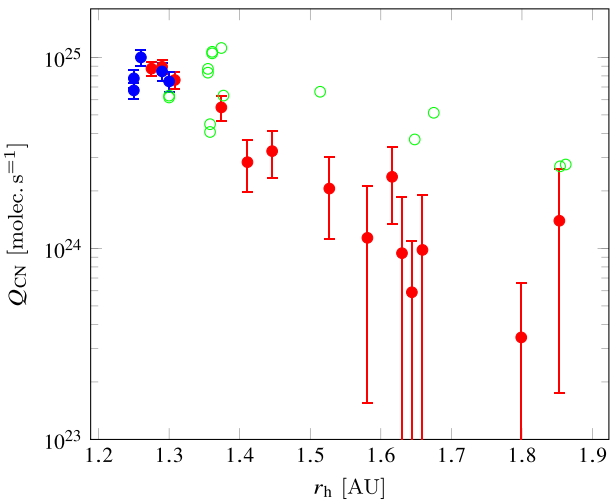

Figure 6. Post-perihelion CN production rates in comet 67P as a function of heliocentric distance with 1σ uncertainties. Red symbols are measurements by LOTUS, blue from TRAPPIST, and green are points from previous orbits from Schleicher (2006).

different from the steep decrease in total brightness from the dust photometry described above.

4 DISCUSSION

If we compare the photometry with predictions from a simple thermophysical model (Meech & Svoreň 2004) we find a reasonable agreement (Fig. 7), but there are differences. In this case, we plot the photometry measured within a fixed radius aperture ($\rho = 5$ arcsec) for comparison with the model output, which already includes corrections for changing observation geometry. The match is good close to perihelion, although this model predicts that there should have been more dust lifted by the gas pre-perihelion. It is interesting to compare this with the fits to previous apparitions (Snodgrass et al.

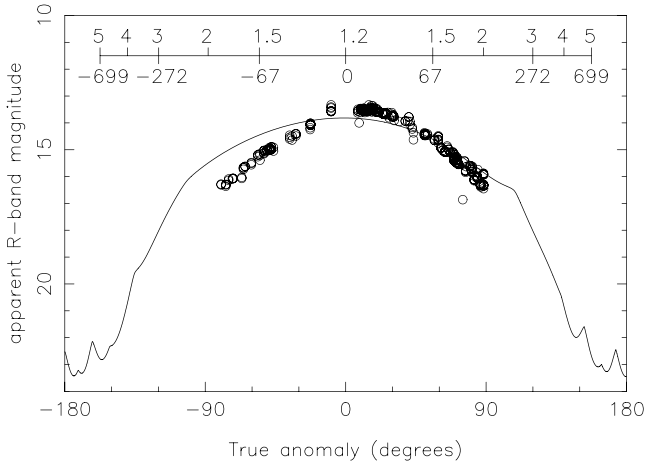

Figure 7. Comparison of photometry (within $\rho = 5$ arcsec aperture) with simple thermophysical model. The upper bar shows r and ΔT (in au and days, respectively).

2013, fig. 9), where this model gave a very good fit to all data apart from the few points closest to perihelion. The model required an active surface area of 1.4 per cent (of the area of a spherical nucleus), and previously needed an enhancement (to 4 per cent) to match the near perihelion points, while this apparition shows a smoothly varying total brightness through perihelion. As the coverage of the perihelion period is much more dense in our data set than for previous apparitions, this could be used to improve the outgassing model – it is worth repeating that the model shown in Fig. 7 is simply an extrapolation of the earlier fit, and has not been adjusted to try to fit the data set plotted here.

Fig. 6 indicates that although there is some scatter in the measured CN production rates, Q(CN) was systematically lower in 2015 than during the 1982/1983 and 1995/1996 post-perihelion apparitions, as measured via narrow-band photometry by Schleicher (2006). It is important to note that the TRAPPIST photometry just after perihelion agrees with the LOTUS spectroscopy. Therefore, this appears to be a real change and not caused by any differences between analysing narrow-band aperture photometry and long-slit spectroscopy. However, with these data alone we cannot associate this with a secular decrease in outgassing rate.

It appears that the CN production rate follows a different pattern than the total dust production, both in terms of similarity to previous orbits and the symmetry around the peak – a longer term view, including observations pre-perihelion and at larger distance post-perihelion with larger aperture telescopes (VLT/FORS), will allow this to be investigated in more detail (Opitom et al in preparation). The period covered by our TRAPPIST and LOTUS observations corresponds to the time when the total brightness matches the model from gas production (Fig. 7), even though they suggest lower total CN production at this time. CN production was even lower pre-perihelion (Opitom et al., in preparation), suggesting that the lower-than-predicted brightness there could be related to lower gas production in this period, but CN is a minor component of the coma; total water production measurements from a variety of Rosetta instruments show a more symmetrical pattern that resembles the total dust production seen in Fig. 4 (Hansen et al. 2016). Instead, the difference in total CN production may be related to different seasonal illumination of the nucleus.

Although there is some indication that the gas production rate is variable from orbit to orbit, the total dust production remains very stable. Further remote observations also support the idea that the activity of the comet is quite stable, in particular as the structure of the coma. Observations from the Wendelstein Observatory in Germany show the same large-scale structures (jets) as were seen in previous orbits (Vincent et al. 2013; Boehnhardt et al. 2016), indicating that the global activity pattern is similar, and the pole position has not significantly changed. Higher resolution polarimetric imaging with the *Hubble Space Telescope* also reveals the same jet structures (Hadamcik et al. 2016).

The robotic telescopes provided a very dense monitoring of the comet activity around perihelion, and therefore gave the best chance to detect small outbursts. We do not see any convincing evidence for outbursts in this data set, and we did not detect in our *r*-band photometry any of the many small 'outbursts' detected by Rosetta (Vincent et al. 2016). This underlines the fact that ground-based photometry naturally 'smears out' the underlying short-time-scale activity of the nucleus, due to the photometric apertures containing both the outflowing dust coma generated from the entire nucleus over several hours or days, plus any underlying slow moving gravitationally bound dust particles. Given the previous spacecraft detections of multiple small outbursts, i.e. A'Hearn et al. (2005), it is possible that the majority of comets undergo continuous small outbursts that fail to be detected even with systematic monitoring as described in this paper.

5 CONCLUSIONS

We present photometry and spectroscopy of 67P around its 2015 perihelion passage, acquired with robotic telescopes. These telescopes (the 2-m LT, 1.2-m STELLA, 0.6-m TRAPPIST and 1-m and 2-m telescopes in the LCOGT network) were able to perform very regular observation despite the challenging observing geometry (low solar elongation). We find the following.

(i) The total brightness of the comet varies smoothly through perihelion, with a peak ~ 2 weeks after closest approach to the Sun.

(ii) The *R*-band brightness largely follows the prediction from Snodgrass et al. (2013), indicating that the dust activity level does not change significantly from orbit to orbit.

(iii) The dust brightness variation is quite symmetrical around its peak, and drops off fairly quickly post-perihelion.

(iv) The gas production (measured in CN) drops off smoothly and slowly post-perihelion.

(v) There is evidence of a decrease in the production rate of CN between the 1980s/1990s and the current apparition, although this needs to be confirmed with observations over a longer period with large telescopes.

ACKNOWLEDGEMENTS

This work was based, in part, on observations conducted at Canary Island telescopes under CCI ITP programme 2015/06, including use of the Liverpool and STELLA telescopes. The Liverpool Telescope is operated on the island of La Palma by Liverpool John Moores University in the Spanish Observatorio del Roque de los Muchachos of the Instituto de Astrofísica de Canarias with financial support from the UK Science and Technology Facilities Council (STFC). The STELLA robotic telescopes in Tenerife are an AIP facility jointly operated by AIP and IAC. TRAPPIST is a project funded by the Belgian Fund for Scientific Research (Fonds National de la Recherche Scientifique, FRS-FNRS) under grant FRFC 2.5.594.09.F, with the participation of the Swiss National Science Foundation (SNF). CS was supported by an STFC Rutherford fellowship. CO acknowledges the support of the FNRS. EJ is an FNRS Research Associate and JM is the Research Director of the FNRS. AF acknowledges support from STFC grant ST/L000709/1. KM acknowledges support from NSF grant AST1413736. ACLR acknowledges partial support from CNES.

REFERENCES

A'Hearn M. F., Schleicher D. G., Millis R. L., Feldman P. D., Thompson D. T., 1984, AJ, 89, 579
A'Hearn M. F., Millis R. L., Schleicher D. G., Osip D. J., Birch P. V., 1995, Icarus, 118, 223
A'Hearn M. F. et al., 2005, Science, 310, 258
Barnsley R. M., Smith R. J., Steele I. A., 2012, Astron. Nachr., 333, 101
Bertin E., 2006, in Gabriel C., Arviset C., Ponz D., Enrique S., eds, ASP Conf. Ser. Vol. 351, Astronomical Data Analysis Software and Systems XV. Astron. Soc. Pac., San Francisco, p. 112
Bertin E., Arnouts S., 1996, A&AS, 117, 393
Bilir S., Ak S., Karaali S., Cabrera-Lavers A., Chonis T. S., Gaskell C. M., 2008, MNRAS, 384, 1178
Boehnhardt H., Riffeser A., Kluge M., Ries C., Schmidt M., Hopp U., 2016, MNRAS, Suppl. 1, in press
Boroson T. et al., 2014, in Peck A. B., Benn C. R., Seaman R. L., eds, Proc. SPIE Conf. Ser. Vol. 9149, Observatory Operations: Strategies, Processes, and Systems V. SPIE, Bellingham, p. 91491E
Brown T. M. et al., 2013, PASP, 125, 1031
Capaccioni F. et al., 2015, Science, 347, 628
Farnham T. L., Schleicher D. G., A'Hearn M. F., 2000, Icarus, 147, 180
Fornasier S. et al., 2015, A&A, 583, A30
Giorgini J. D., 2015, NASA JPL Horizons On-Line Ephemeris System. Available at http://ssd.jpl.nasa.gov/?horizons
Hadamcik E., Levasseur-Regourd A.-C., Hines D. C., Sen A., Lasue J., Renard J.-B., 2016, MNRAS, Suppl. 1, in press
Hansen K. C. et al., 2016, MNRAS, Suppl. 1, in press
Haser L., 1957, Bull. Soc. R. Sci. Liege, 43, 740
Holmberg J., Flynn C., Portinari L., 2006, MNRAS, 367, 449
Jehin E. et al., 2011, The Messenger, 145, 2
Jenness T., Economou F., 2015, Astron. Comput., 9, 40
Jester S. et al., 2005, AJ, 130, 873
Le Roy L. et al., 2015, A&A, 583, A1
Luspay-Kuti A. et al., 2015, A&A, 583, A4
Marcus J. N., 2007, Int. Comet Q., 29, 119
Meech K. J., Svoreň J., 2004, in Festou M. C., Keller H. U., Weaver H. A., eds, Comets II. Univ. Arizona Press, Tucson, p. 317
Opitom C., Jehin E., Manfroid J., Hutsemékers D., Gillon M., Magain P., 2015, A&A, 574, A38
Piascik A. S., Steele I. A., Bates S. D., Mottram C. J., Smith R. J., Barnsley R. M., Bolton B., 2014, in Ramsay S. K., McLean I. S., Takami H., eds, Proc. SPIE Conf. Ser. Vol. 9147, Ground-based and Airborne Instrumentation for Astronomy V. SPIE, Bellingham, p. 91478H
Roeser S., Demleitner M., Schilbach E., 2010, AJ, 139, 2440
Schleicher D. G., 2006, Icarus, 181, 442
Schleicher D. G., 2010, AJ, 140, 973
Schleicher D. G., Millis R. L., Birch P. V., 1998, Icarus, 132, 397
Snodgrass C., Tubiana C., Bramich D. M., Meech K., Boehnhardt H., Barrera L., 2013, A&A, 557, A33
Snodgrass C. et al., 2016, A&A, 588, A80
Steele I. A. et al., 2004, in Oschmann J. M., Jr, ed., Proc. SPIEConf. Ser. Vol. 5489, Ground-based Telescopes. SPIE, Bellingham, p. 679
Steele I. A., Mottram C. J., Smith R. J., Barnsley R. M., 2014, in Holland A. D., Beletic J., eds, Proc. SPIEConf. Ser. Vol. 9154, High Energy,

Optical, and Infrared Detectors for Astronomy VI. SPIE, Bellingham, p. 915428
Steele I. A. et al., 2016, MNRAS, 460, 4268
Strassmeier K. G. et al., 2004, Astron. Nachr., 325, 527
Strassmeier K. G. et al., 2010, Adv. Astron., 2010, 970306
Vincent J.-B., Lara L. M., Tozzi G. P., Lin Z.-Y., Sierks H., 2013, A&A, 549, A121
Vincent J.-B. et al., 2016, MNRAS, Suppl. 1, in press
Zacharias N., Finch C. T., Girard T. M., Henden A., Bartlett J. L., Monet D. G., Zacharias M. I., 2013, AJ, 145, 44

SUPPORTING INFORMATION

Additional Supporting Information may be found in the online version of this article:

Tables 1 and A1 are also available at the CDS via anonymous ftp to cdsarc.u-strasbg.fr (130.79.128.5) or via http://cdsarc.u-strasbg.fr/viz-bin/qcat?J/MNRAS/VOL/PAGE

tables.tgz
(http://www.mnras.oxfordjournals.org/lookup/suppl/doi:10.1093/mnras/stw2300/-/DC1).

Please note: Oxford University Press is not responsible for the content or functionality of any supporting materials supplied by the authors. Any queries (other than missing material) should be directed to the corresponding author for the article.

APPENDIX A: PHOTOMETRY

This appendix gives all *R*-band photometry from the robotic telescopes mentioned in this paper. All values are based on an aperture with radius $\rho = 10\,000$ km at the distance of the comet. Where the telescopes used an SDSS-*r* filter, a colour correction of −0.2105 has been applied. Heliocentric distance (r) and time from perihelion (ΔT) are given, together with the apparent magnitude as well as the magnitude corrected to unit geocentric distance and zero phase angle, using $\beta = 0.02$ mag deg^{-1}. The $Af\rho$ quantity is given in cm, without any correction for phase angle in this case.

Table A1. *R*-band photometry. Measured within an aperture with radius ρ 10 000 km. Full table is available online, first five rows given as an example.

UT date	r (au)	ΔT (d)	Mag	$R(r,1,0)$	$Af\rho$ (cm)	Tel./inst.
04-18.41	1.83	−116.68	16.280	13.859	94.3	TRAPPIST
04-18.42	1.83	−116.67	16.310	13.889	91.7	TRAPPIST
04-25.41	1.78	−109.68	16.230	13.846	87.4	TRAPPIST
04-25.42	1.78	−109.67	16.160	13.776	93.2	TRAPPIST
04-25.42	1.78	−109.67	16.210	13.826	89.0	TRAPPIST
...	...	...	...	...	...	...

This paper has been typeset from a TEX/LATEX file prepared by the author.